www.nature.com/cmi

ARTICLE

The deubiquitinase OTUD1 inhibits colonic inflammation by suppressing RIPK1-mediated NF-κB signaling

Bo Wu[1,5], Lihua Qiang[2,3,5], Yong Zhang[1,2,5], Yesheng Fu[1,5], Mengyuan Zhao[2,3], Zehui Lei[2,3], Zhe Lu[2,3], Yan-Ge Wei[1], Hongmiao Dai[1], Yingwei Ge[1], Mingqiu Liu[1], Xuemei Zhou[1], Zhiqiang Peng[1], Hongchang Li[1], Chun-Ping Cui[1], Jing Wang[2], Hui Zheng[4], Cui Hua Liu[2,3]✉ and Lingqiang Zhang[1]✉

The E3 ubiquitin ligase (E3)-mediated ubiquitination and deubiquitinase (DUB)-mediated deubiquitination processes are closely associated with the occurrence and development of colonic inflammation. Ovarian tumor deubiquitinase 1 (OTUD1) is involved in immunoregulatory functions linked to infectious diseases. However, the effect of OTUD1 on intestinal immune responses during colonic inflammatory disorders such as inflammatory bowel disease (IBD) remains unclear. Here, we show that loss of OTUD1 in mice contributes to the pathogenesis of dextran sulfate sodium (DSS)-induced colitis via excessive release of proinflammatory cytokines. In addition, bone marrow transplantation experiments revealed that OTUD1 in hematopoietic cells plays a dominant role in protection against colitis. Mechanistically, OTUD1 physically interacts with receptor-interacting serine/threonine-protein kinase 1 (RIPK1) and selectively cleaves K63-linked polyubiquitin chains from RIPK1 to inhibit the recruitment of NF-κB essential modulator (NEMO). Moreover, the expression of OTUD1 in mucosa samples from ulcerative colitis (UC) patients was lower than that in mucosa samples from healthy controls. Furthermore, we demonstrate that the UC-associated OTUD1 G430V mutation abolishes the ability of OTUD1 to inhibit RIPK1-mediated NF-κB activation and intestinal inflammation. Taken together, our study unveils a previously unexplored role of OTUD1 in moderating intestinal inflammation by inhibiting RIPK1-mediated NF-κB activation, suggesting that the OTUD1-RIPK1 axis could be a potential target for the treatment of IBD.

Keywords: OTUD1; RIPK1; NF-κB; IBD

Cellular & Molecular Immunology (2022) 19:276–289; https://doi.org/10.1038/s41423-021-00810-9

INTRODUCTION

Inflammatory bowel diseases (IBDs), including Crohn's disease (CD) and ulcerative colitis (UC), are complex multifactorial diseases characterized by chronic and relapsing inflammation and dysregulated immune responses in the gastrointestinal tract [1]. It has been reported that multiple immune cell populations, including macrophages, dendritic cells (DCs), neutrophils and eosinophils, present in the intestinal mucosa contribute to inflammation by secreting proinflammatory cytokines, including tumor necrosis factor (TNF), interleukin (IL)-6 and IL-1β, during IBD. In addition, intestinal epithelial cells play important roles in modulating gut immune homeostasis by maintaining the integrity of intestinal mucosal barriers and regulating the functions of intestinal immune cells [2]. Thus, investigating the precise regulatory mechanisms that control innate immune responses in the intestine is critical to our understanding of IBD pathogenesis.

Ubiquitination is a crucial enzymatic cascade for posttranslational modifications related to the occurrence and development of various inflammatory diseases, including IBD [3, 4], a chronic disorder accompanying immune system dysregulation and dysbiosis [5]. E3 ubiquitin ligase (E3s)-mediated ubiquitination and deubiquitinase (DUB)-mediated deubiquitination are two reversible processes that can target proteins involved in colonic inflammatory signaling pathways. For example, ubiquitin-specific protease 7 (USP7) stabilizes a forkhead lineage transcription factor (Foxp3) and increases the suppressive capacity of Treg cells- to alleviate intestinal inflammation [6]. Another deubiquitinase, TNF-α-induced protein 3 (TNFAIP3), inhibits myeloid differentiation factor 88 (MyD88)-dependent and MyD88-independent activation of dendritic cells to prevent colitis [7]. Therefore, DUBs are critical for the intestinal immunomodulatory functions of immune cells.

Ovarian tumor deubiquitinase 1 (OTUD1), also called DUBA7 or OTDC1, is a DUB that participates extensively in inflammatory homeostasis to control the progression of various diseases. Previous studies have shown that mutation of OTUD1 exacerbates autoimmune disorders and enhances innate immunity [8]. In addition, OTUD1 modulates the activation of inflammatory signaling pathways and the production of inflammatory cytokines during viral and fungal infections [9, 10]. Moreover, OTUD1 can suppress colon cancer progression by triggering immunogenic

[1]State Key Laboratory of Proteomics, National Center for Protein Sciences (Beijing), Beijing Institute of Lifeomics, Beijing 100850, China. [2]CAS Key Laboratory of Pathogenic Microbiology and Immunology, Institute of Microbiology, Chinese Academy of Sciences, Beijing 100101, China. [3]Savaid Medical School, University of Chinese Academy of Sciences, Beijing 101408, China. [4]International Institute of Infection and Immunity, Institutes of Biology and Medical Sciences, Soochow University, Suzhou, Jiangsu, China. [5]These authors contributed equally: Bo Wu, Lihua Qiang, Yong Zhang, Yesheng Fu. ✉email: liucuihua@im.ac.cn; zhanglq@nic.bmi.ac.cn

Received: 8 July 2021 Revised: 20 November 2021 Accepted: 22 November 2021
Published online: 7 December 2021

cell death [11]. Although OTUD1 has been reported to participate in the coordination of intestinal immune responses, the physiological function and the underlying mechanism of OTUD1 in the maintenance of intestinal homeostasis have not yet been elucidated.

In this study, we show that OTUD1 alleviates intestinal inflammation by impairing proinflammatory cytokine production and that OTUD1 in hematopoietic cells is responsible for the protective effects of OTUD1 against DSS-induced colitis. Furthermore, we revealed that OTUD1 inhibits nuclear factor κB (NF-κB) activation by removing K63-linked polyubiquitin chains from RIPK1, thus suppressing the recruitment of NEMO and the production of proinflammatory cytokines. Taken together, these findings indicate that OTUD1 exhibits an inhibitory effect on RIPK1-mediated NF-κB activation to prevent intestinal inflammation. These results uncover an essential role of OTUD1 in intestinal homeostasis, suggesting that targeting OTUD1 might be a potential therapeutic approach for IBD.

RESULTS

Otud1$^{-/-}$ mice exhibit increased susceptibility to DSS-induced colitis

The approximately 100 human DUBs encoded in the human genome exert various functions by modulating different substrates [12]. To identify pivotal DUBs involved in maintaining immune homeostasis, we screened for DUBs that respond to lipopolysaccharide (LPS) stimulation. Following stimulation, the expression of *OTUD1* was significantly and consistently elevated compared to that of other DUBs (Supplementary Fig. 1; Supplementary Table 1). LPS is a major proinflammatory component of gram-negative bacteria, including enteropathogenic *Escherichia coli* (EPEC) [13]. We then confirmed increases in OTUD1 transcript and protein levels during LPS stimulation and EPEC infection (Fig. 1a; Supplementary Fig. 2a–c). DNA methylation is a critical epigenetic mechanism that controls gene expression [14]. To explore whether DNA methylation modulates the expression of OTUD1 during LPS stimulation, the methylation and expression levels of OTUD1 were determined. We identified two CpG islands (CGIs) in the promoter of OTUD1 (CGI1, 100 base pairs (bp), −721/−622 bp and CGI2, 199 bp, −255/-57 bp; transcription start site = +1; Supplementary Fig. 2d). Methylation-specific PCR also confirmed that LPS treatment induced an increase in the methylation of the OTUD1 promoter (Supplementary Fig. 2e). Moreover, the dual-luciferase reporter assay showed that methylation of the OTUD1 promoter reduced its transcriptional activity (Supplementary Fig. 2f). Furthermore, pretreatment with the DNA methylation inhibitor decitabine promoted LPS-induced OTUD1 transcription (Supplementary Fig. 2g). These findings suggest that LPS-induced hypomethylation of the OTUD1 promoter region contributes to the upregulation of OTUD1. Although a previous study showed that *Otud1*-deficient mice exhibited increased susceptibility to LPS stimulation [15], we further verified that *Otud1*-deficient mice were likely to die from LPS-induced septic shock (Fig. 1b). Taken together, these data suggest that OTUD1 is responsible for maintaining immune homeostasis.

Previous studies have demonstrated that EPEC can efficiently infect the gut mucosa and cause intestinal mucosal dysfunction via release of LPS [16, 17]. As described above, we found that OTUD1 responds to LPS stimulation and EPEC infection, but whether OTUD1 is involved in the intestinal inflammatory response is unknown. To assess the role of OTUD1 in the development of IBD, WT and *Otud1*$^{-/-}$ mice were treated with 2.5% dextran sodium sulfate (DSS), and we found that the transcript level of *Otud1* was increased in a time-dependent manner and that *Otud1* showed the highest expression in colonic tissue on Day 6 after DSS administration (Fig. 1c, d). In the setting of DSS-induced colitis, *Otud1*$^{-/-}$ mice displayed more severe symptoms of intestinal inflammation, as evidenced by their greater body weight loss, greater amount of rectal bleeding and shorter colon length, while *Otud1* deficiency did not lead to intestinal inflammation under physiological conditions (Fig. 1e–h). In addition, histopathological analysis revealed a severely damaged colonic mucosa and extensive infiltration of inflammatory cells in the colons of *Otud1*$^{-/-}$ mice (Fig. 1i), as reflected in the pathological assessment (Fig. 1j). We also isolated the immune cells in the intestinal lamina propria and found that deletion of *Otud1* resulted in significantly increased numbers of multiple immune cells, including dendritic cells (DCs), macrophages and neutrophils, during DSS treatment (Fig. 1k). In addition, *Otud1* knockout did not affect T cell activation or differentiation in mesenteric lymph nodes under physiological conditions (Supplementary Fig. 3). Moreover, immunohistochemical analysis with an anti-CD68 antibody showed significant enrichment of macrophages in colonic tissues from *Otud1*$^{-/-}$ mice compared with those from WT mice after DSS administration, suggesting that macrophages might be involved in the regulation of intestinal inflammation by OTUD1 (Fig. 1l). Taken together, these data suggest that *Otud1*$^{-/-}$ mice are susceptible to DSS-induced colitis.

OTUD1 deficiency promotes proinflammatory cytokine production

The pathological process of IBD is characterized by excessive and chronic intestinal inflammation [18]. It is well established that activation of the NF-κB signaling pathway by LPS is associated with the production of a variety of proinflammatory cytokines, such as TNF-α, IL-6 and IL-1β [19]. To determine whether OTUD1 regulates the production of proinflammatory cytokines, we established stable *OTUD1* knockdown cell lines (Supplementary Fig. 4a). After stimulation with LPS, the transcript and protein levels of IL-6, IL-1β, and TNF-α were much higher in *OTUD1* knockdown cells than in WT cells (Supplementary Fig. 4b–c). In addition, BMDMs isolated from *Otud1*$^{-/-}$ mice produced more *Il-6, Il-1b*, and *Tnf-α* when stimulated with LPS than BMDMs isolated from WT mice (Fig. 2a), with higher levels of Il-6 and Tnf-α in the cell supernatants (Fig. 2b). These data indicate that OTUD1 deficiency promotes inflammatory responses. Consistent with this result, we found that the transcript and protein levels of Il-6, Il-1b, and Tnf-α were significantly increased in the colons of *Otud1*$^{-/-}$ mice after DSS treatment (Fig. 2c, d). Collectively, these data demonstrate that OTUD1 inhibits intestinal inflammation by suppressing proinflammatory cytokine production.

OTUD1 in hematopoietic cells is responsible for protection against DSS-induced colitis

Since intestinal immune cells, including macrophages, DCs and neutrophils, are mostly derived from hematopoietic cells in the bone marrow, we generated bone marrow chimeric mice via adoptive transfer of bone marrow to determine whether bone marrow-derived cells are involved in the protective effects of OTUD1 against colitis (Fig. 3a). Flow cytometric analysis using the congenic surface markers CD45.1 and CD45.2 showed that >90% of the cells in the chimeric mice were donor cells (Fig. 3b). Consistent with the observations in the conventional *Otud1*$^{-/-}$ mice, the mice in the *Otud1*$^{-/-}$ autotransplantation (*Otud1*$^{-/-}$ > *Otud1*$^{-/-}$) group presented a more severe colitis phenotype than those in the WT autotransplantation (WT > WT) group. The group of WT mice receiving *Otud1*$^{-/-}$ bone marrow (*Otud1*$^{-/-}$ > WT group) and mice in the *Otud1*$^{-/-}$ > *Otud1*$^{-/-}$ group exhibited more severe symptoms of colitis, along with greater body weight loss, more rectal bleeding, a shorter colon length and deteriorated colonic inflammatory histopathology, relative to mice in the WT > WT group and the group of *Otud1*$^{-/-}$ mice receiving WT bone marrow (WT > *Otud1*$^{-/-}$ group) (Fig. 3c–h). Consistent with this finding, colonic tissues from mice in the *Otud1*$^{-/-}$>WT and *Otud1*$^{-/-}$ > *Otud1*$^{-/-}$ groups exhibited higher levels of

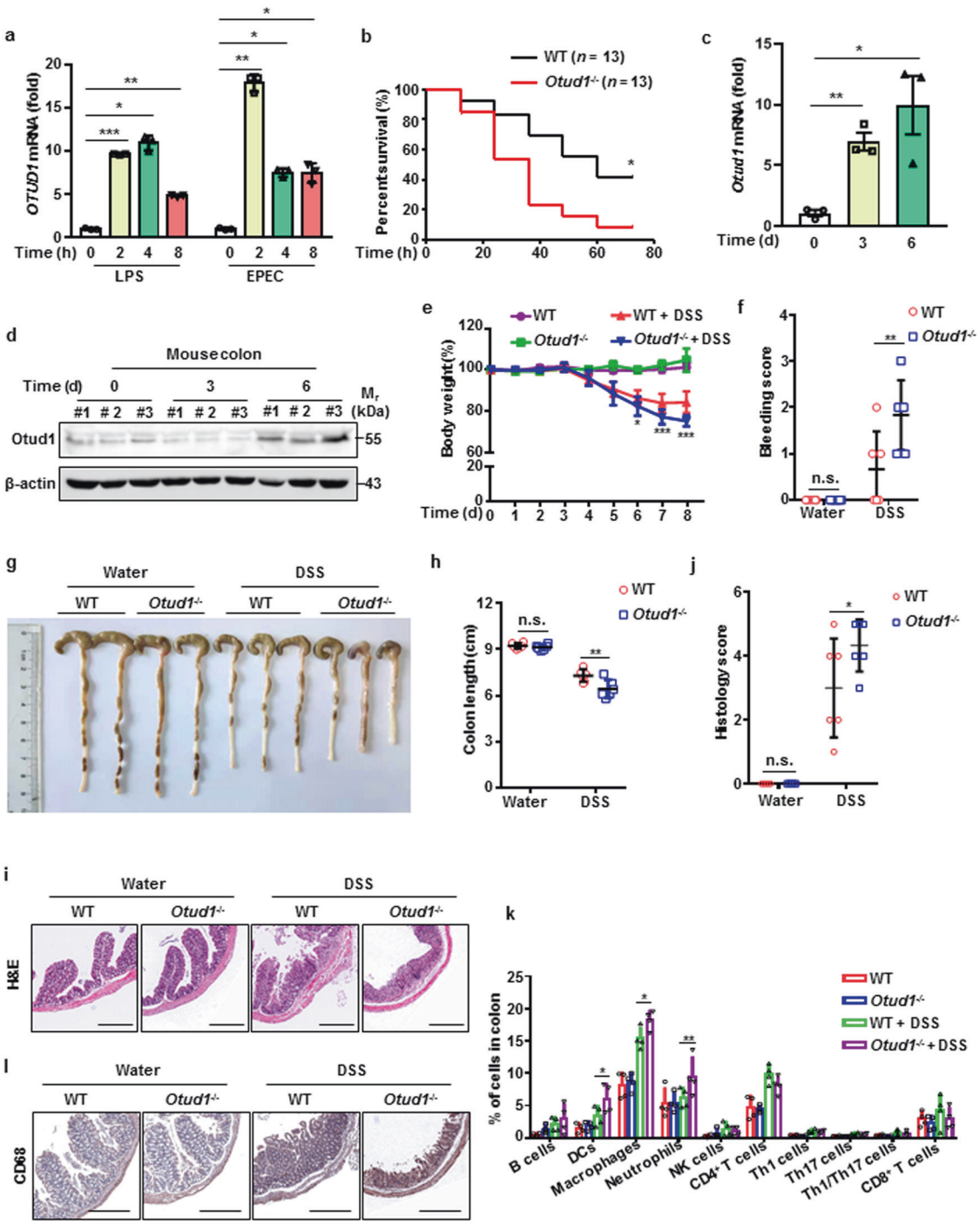

Fig. 1 *Otud1*$^{-/-}$ mice are susceptible to DSS-induced colitis. **a** Quantitative PCR analysis of *OTUD1* mRNA expression in PMA-stimulated U937 cells (1×10^6) challenged with LPS (100 ng/mL) or infected with EPEC (MOI = 150) for the indicated time points. **b** Survival (Kaplan–Meier) curves of WT and *Otud1*$^{-/-}$ mice injected i.p. with LPS (25 mg/kg) for 80 h. The *P* value for percent survival was calculated using the log-rank test. **c** Quantitative PCR analysis of *Otud1* mRNA expression in the colons of mice treated with 2.5% DSS ($n = 3$ for each timepoint). **d** Immunoblot analysis of Otud1 expression in the colons of mice treated with 2.5% DSS ($n = 3$ for each timepoint). **e** Body weight of WT ($n = 6$) and *Otud1*$^{-/-}$ mice ($n = 6$) exposed to 2.5% DSS for 6 days and then provided regular drinking water for 2 days. **f** Bleeding score of colonic tissue from mice on Day 5 after initiation of DSS administration. **g**, **h** The colon length in WT and *Otud1*$^{-/-}$ mice on Day 8 after initiation of DSS administration. **i** Representative images of H&E-stained colon sections from WT and *Otud1*$^{-/-}$ mice following DSS administration. Scale bar: 500 μm. **j** Semiquantitative histological scores of colon sections from WT and *Otud1*$^{-/-}$ mice. **k** Flow cytometric analysis of the number of various immune cells among CD45+ cells from the intestinal lamina propria of WT and *Otud1*$^{-/-}$ mice following DSS administration. **l** Representative images of CD68 staining in colonic tissues from WT and *Otud1*$^{-/-}$ mice following DSS administration. Scale bar: 500 μm. These data are presented as a representative mean ± SD of three independent biological replicates. *$P < 0.05$; **$P < 0.01$; ***$P < 0.001$

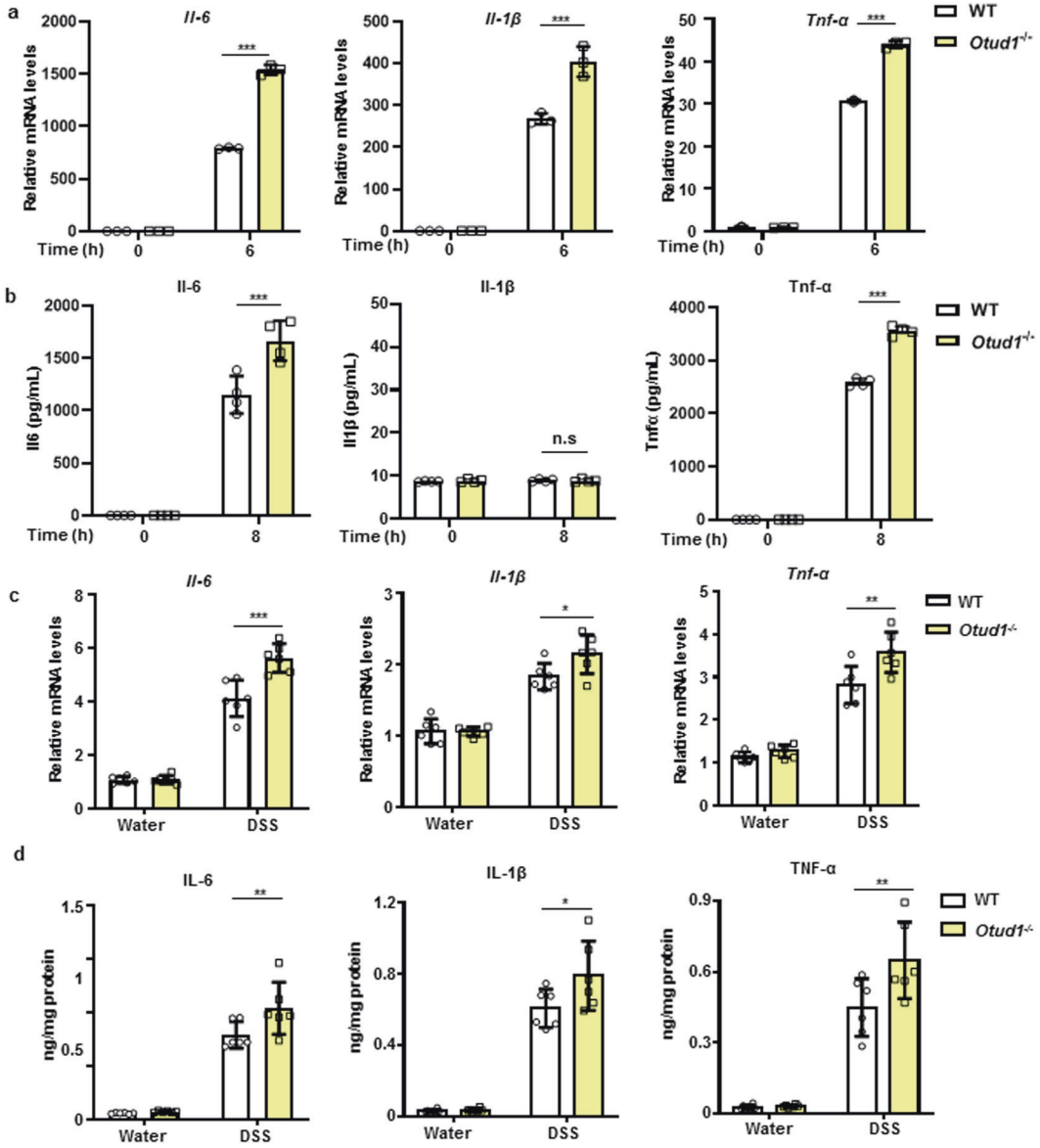

Fig. 2 OTUD1 deficiency promotes the production of proinflammatory cytokines. **a** Quantitative PCR analysis of *Il-6*, *Il-1b*, and *Tnf-α* mRNA expression in WT and *Otud1*$^{-/-}$ BMDMs (1×10^6) treated with LPS (100 ng/mL). **b** ELISA of the production of Il-6, Il-1b, and Tnf-α in supernatants from WT and *Otud1*$^{-/-}$ BMDMs (1×10^6) treated with LPS (100 ng/mL). **c** Quantitative PCR analysis of *Il-6*, *Il-1b*, and *Tnf-α* mRNA expression in colon sections from WT and *Otud1*$^{-/-}$ mice treated with 2.5% DSS. **d** ELISA of the production of Il-6, Il-1b, and Tnf-α in colon sections from WT and *Otud1*$^{-/-}$ mice treated with 2.5% DSS. The graph shows a representative mean ± SD of three or four independent biological replicates. *$P < 0.05$; ***$P < 0.001$; n.s not significant

proinflammatory cytokines, including Il-6, Il-1β, and Tnf-α, than colonic tissues from mice in the WT > WT and WT > *Otud1*$^{-/-}$ groups (Fig. 3i, j). These findings indicate that OTUD1 expression in hematopoietic cells is responsible for mediating resistance to DSS-induced colitis through suppression of proinflammatory cytokine production.

OTUD1 inhibits the NF-κB signaling pathway by interacting with RIPK1

The NF-κB signaling pathway is activated by a wide variety of stimuli, such as TNF-α, LPS and poly(I:C). Previous studies have reported that OTUD1 inhibits NF-κB signaling pathway activation triggered by poly(I:C) [8, 10]. A recent study revealed that OTUD1 promotes C-type lectin receptor (CLR)-mediated NF-κB activation [9]. However, the roles and regulatory mechanisms of OTUD1 in LPS-induced NF-κB activation remain unclear. To determine the function of OTUD1 in LPS-induced NF-κB signaling pathway activation, we stimulated WT and OTUD1-overexpressing cells with LPS and found that OTUD1 overexpression significantly suppressed the NF-κB signaling pathway (Fig. 4a). As expected, OTUD1 knockdown U937 cells exhibited increased phosphorylation of p65 and IκBα compared with that in WT U937 cells following LPS stimulation (Fig. 4b). Therefore, OTUD1 exerts an inhibitory effect on LPS-induced NF-κB activation.

Various signaling molecules, including myeloid differentiation primary response protein 88 (MyD88), interleukin-1 receptor associated kinase 1 (IRAK1), TIR domain-containing adaptor inducing interferon-β (TRIF), RIPK1, IκB kinase α (IKKα), TGF-β activated kinase 1 (TAK1) and TAK1-binding protein 2 (TAB2), are required for activation of NF-κB signaling pathways [20]. Here, we

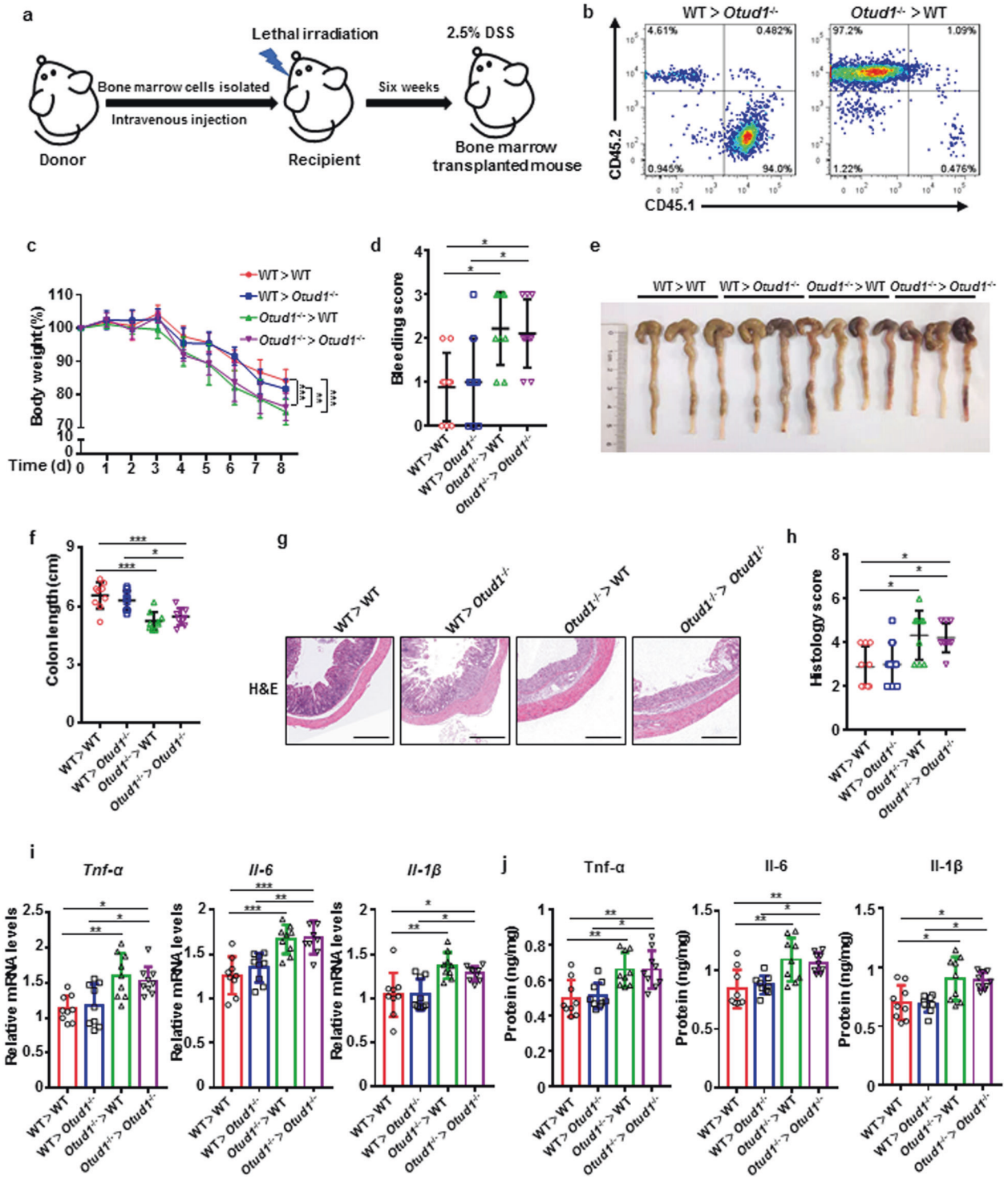

Fig. 3 OTUD1 in hematopoietic cells plays a dominant role in preventing DSS-induced colitis. **a** Schematic representation of chimeric recipient mice that were generated by transplanting equal numbers of WT (CD45.1) and *Otud1*$^{-/-}$ (CD45.2) bone marrow cells into lethally irradiated recipient mice. **b** Representative flow cytometry plots of CD45.1^{+} and CD45.2^{+} bone marrow cells in mice 6 weeks after reconstitution. **c** Body weight of bone marrow chimeric mice exposed to 2.5% DSS for 6 days and then provided regular drinking water for 2 days. **d** Bleeding score of colonic tissue from bone marrow chimeric mice on Day 5 after DSS administration. **e**, **f** The colon length in bone marrow chimeric mice on Day 8 after initiation of DSS administration. **g** Representative images of H&E-stained colon sections from bone marrow chimeric mice after DSS administration. Scale bar: 500 μm. **h** Semiquantitative histological scores of colon sections from bone marrow chimeric mice. **i** Quantitative PCR analysis of *Il-6*, *Il-1b*, and *Tnf-α* mRNA expression in colon sections from bone marrow chimeric mice treated with 2.5% DSS. **j** ELISA of the production of Il-6, Il-1b, and Tnf-α in colon sections from bone marrow chimeric mice treated with 2.5% DSS. WT > WT, $n = 9$; WT > *Otud1*$^{-/-}$, $n = 9$; *Otud1*$^{-/-}$ > *Otud1*$^{-/-}$, $n = 9$; *Otud1*$^{-/-}$ > WT, $n = 9$. The graph shows a representative mean ± SD of three independent biological replicates. *$P < 0.05$; ***$P < 0.001$; n.s not significant

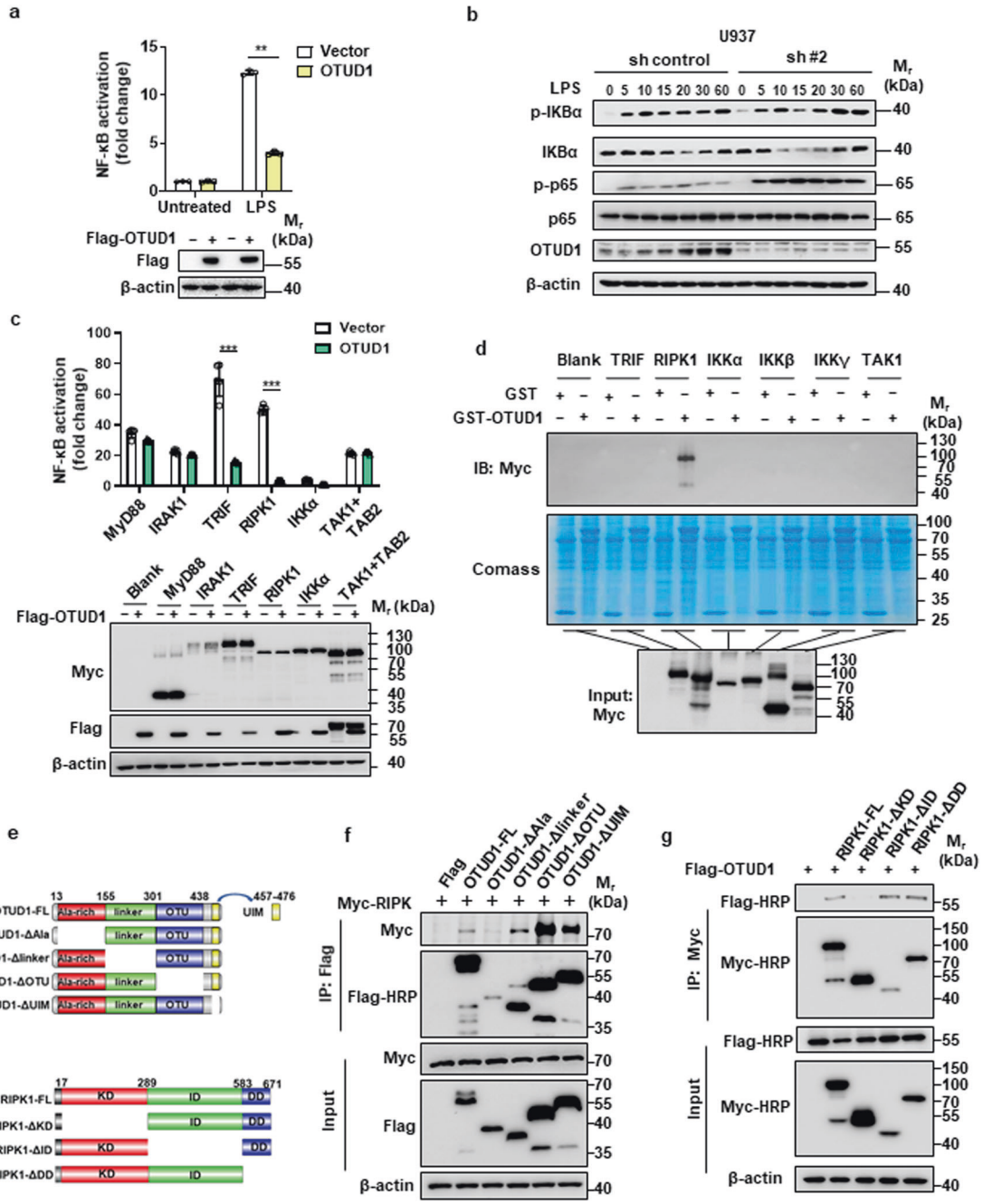

Fig. 4 OTUD1 inhibits the activation of the NF-κB signaling pathway by binding to RIPK1. **a** Luciferase assay of NF-κB activity in 293/hTLR4A-MD2-CD14 cells treated with LPS for 12 h after transfection with control or OTUD1 vector together with the NF-κB reporter vector and CMV-driven Renilla luciferase vector for 36 h. **b** Immunoblot analysis of the protein levels of p-p65, p65, p-IKBα, IKBα, OTUD1 and β-actin in U937 knockdown cells (2×10^6) challenged with LPS (100 ng/mL) for the indicated times. **c** Luciferase assay of NF-κB activity in HEK293T cells transfected with reporter plasmids, empty vector, or the Flag-OTUD1 plasmid together with MyD88, IRAK1, TRIF, RIPK1, IKKα or TAK1/TAB2 at 24 h post transfection. **d** Precipitation of TRIF, RIPK1, IKKα, IKKβ, IKKγ and TAK1 by GST-OTUD1. **e** Domain mapping of OTUD1 and RIPK1. **f** Immunoblot analysis of proteins immunoprecipitated with an anti-Flag antibody from lysates of HEK293T cells transfected with truncations of OTUD1. **g** Immunoblot analysis of proteins immunoprecipitated with an anti-Myc antibody from lysates of HEK293T cells transfected with truncations of RIPK1. These data are presented as a representative mean ± SD of three independent biological replicates. *$P < 0.05$; **$P < 0.01$; ***$P < 0.001$

found that OTUD1 suppressed NF-κB signaling pathway activation mediated by TRIF and RIPK1 but not that mediated by MyD88, IRAK1, IKKα or TAK1/TAB2 (Fig. 4c). We then transfected Flag-tagged OTUD1 into HEK-293T cells to identify the interacting proteins of OTUD1 by mass spectrometry. RIPK1, which is involved in the NF-κB signaling pathway, was identified as an interacting partner of OTUD1 (Supplementary Fig. 5a; Supplementary Table 2). We further demonstrated that OTUD1 specifically interacted with RIPK1 and not with TRIF, IKKα, IKKβ, IKKγ or TAK1 (Fig. 4d). Then, the interaction between OTUD1 and RIPK1 was confirmed by coimmunoprecipitation and GST pulldown assays (Supplementary Fig. 5b, c). Moreover, we performed immunofluorescence and

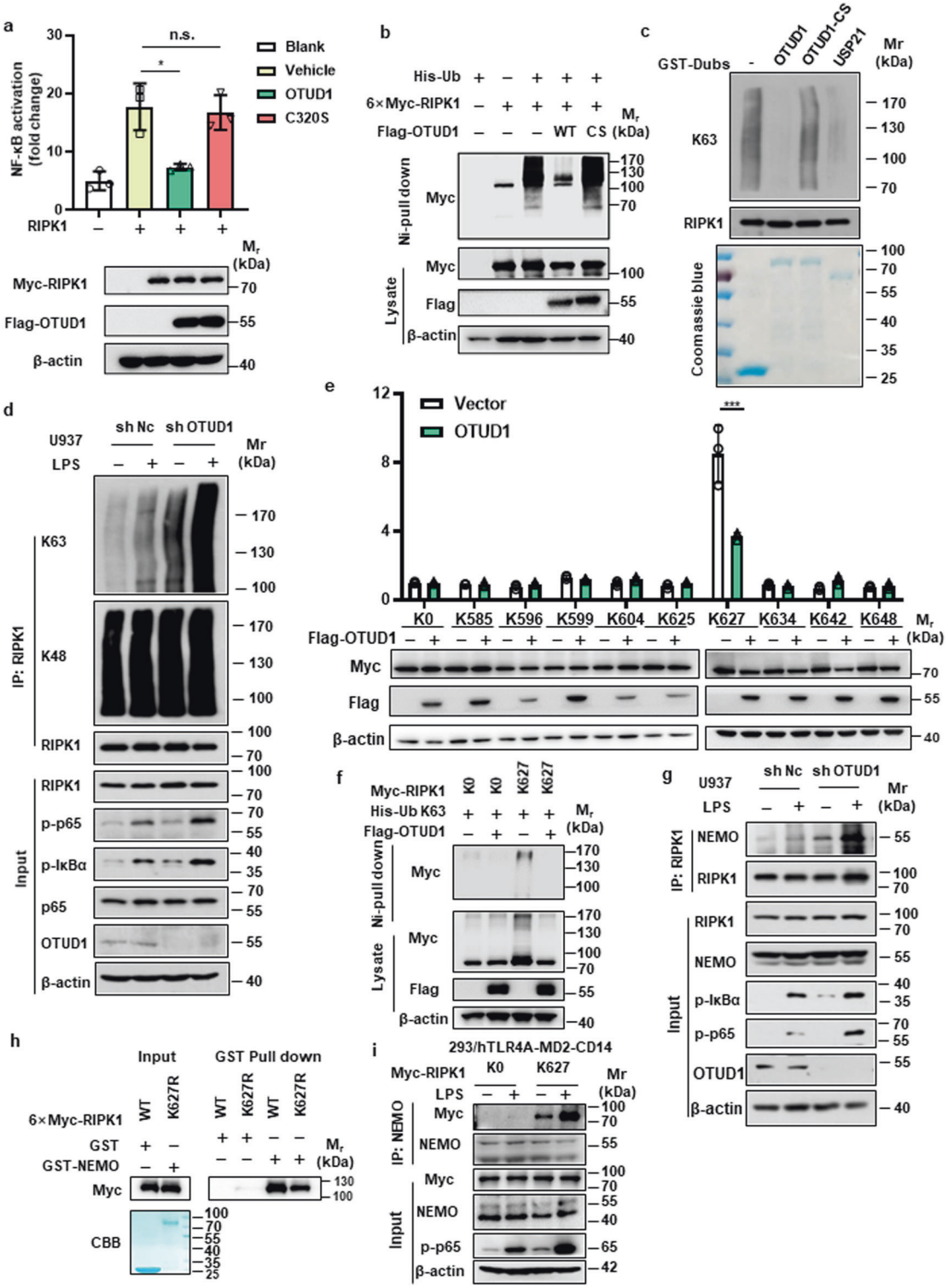

Fig. 5 OTUD1 deubiquitinates RIPK1. **a** Luciferase assay to evaluate the effects of OTUD1 and OTUD1 (C320S) on RIPK1-mediated activation of the NF-κB pathway. **b** Immunoblot analysis of RIPK1 polyubiquitination in cells transfected with Flag-OTUD1 or Flag-OTUD1 (C320S). **c** In vitro assay of RIPK1 deubiquitination by OTUD1, OTUD1 C320S and USP21. **d** Immunoblot analysis of RIPK1 ubiquitination and p65 and IκBα phosphorylation in U937 cells transfected with negative control and OTUD1 shRNA following LPS stimulation at the indicated time points. **e** Luciferase assay of NF-κB activity in HEK293T cells transfected with RIPK1 or various RIPK1 lysine-only mutants. **f** Immunoblot analysis of RIPK1 K63-linked polyubiquitination in HEK293T cells transfected with RIPK1 K0, RIPK1 K627 or OTUD1. **g** Immunoblot analysis of RIPK1 and NEMO in U937 cells transfected with negative control and OTUD1 shRNA following LPS stimulation at the indicated time points. **h** Immunoblot analysis of WT RIPK1 and RIPK1 K627R pulled down with NEMO in the GST pulldown assay. **i** Immunoblot analysis of RIPK1 mutants pulled down with NEMO in 293/hTLR4A-MD2-CD14 cells transfected with the RIPK1 K0 or RIPK1 K627 mutant following LPS stimulation. The graph shows a representative mean ± SD of three independent biological replicates. *$P < 0.05$; ***$P < 0.001$; n.s not significant

immunoprecipitation assays and demonstrated that the association of OTUD1 with RIPK1 was independent of LPS stimulation (Supplementary Fig. 5d–f). To identify the specific domains required for the interaction of OTUD1 with RIPK1, we constructed a series of truncation mutants and found that the Ala-rich domain of OTUD1 was essential for interaction with the kinase domain (KD) of RIPK1 (Fig. 4e–g). These results suggest that RIPK1 is critical for OTUD1-mediated suppression of LPS-induced NF-κB activation.

OTUD1 reverses K63-linked ubiquitination of RIPK1

OTUD1 regulates multiple cellular processes in a manner dependent on its deubiquitinase activity [10, 21]. A previous study reported that a catalytically dead OTUD1 mutant (C320S) could not inhibit NF-κB pathway activation stimulated by poly(I: C) [8]. We found that OTUD1 but not the OTUD1 (C320S) mutant inhibited NF-κB pathway activation induced by RIPK1 (Fig. 5a) and that OTUD1 deubiquitinated RIPK1 in a manner dependent on its enzyme activity (Fig. 5b, c). To determine which type of ubiquitin chain on RIPK1 is affected by OTUD1, we performed deubiquitination assays with a series of ubiquitin mutants and revealed that OTUD1 removed K48- and K63-linked ubiquitin chains from RIPK1 (Supplementary Fig. 6a). However, OTUD1 deficiency dramatically increased K63-linked but not K48-linked ubiquitination of RIPK1, accompanied by increased phosphorylation of p65 and IκBα, during LPS treatment (Fig. 5d). In addition, OTUD1 deficiency did not affect RIPK1 protein stability regardless of LPS stimulation (Supplementary Fig. 6b–d). These findings suggest that OTUD1-specifically removes K63-linked polyubiquitin chains from RIPK1 during LPS stimulation.

To further identify the ubiquitination sites in RIPK1 regulated by OTUD1, we constructed a series of RIPK1 mutants, including a K-all-R mutant lacking intact lysines (K0) and three lysine-only mutants retaining lysine residues within the kinase domain (KD-Ks), linker domain (ID-Ks) or death domain (DD-Ks) of RIPK1. The results showed that lysine residues in the RIPK1 death domain were essential for RIPK1-mediated NF-κB activation, which was significantly inhibited by OTUD1 (Supplementary Fig. 6e, f). We further constructed nine lysine-only mutants of the RIPK1 death domain and demonstrated that K627 in the death domain of RIPK1 was indispensable for the activation of the NF-κB pathway (Fig. 5e). Consistent with this finding, the ability of the RIPK1 K627R mutant to induce the activation of the NF-κB pathway was attenuated (Supplementary Fig. 6g). Moreover, K63-linked ubiquitination of RIPK1 at the lysine 627 residue could be reversed by OTUD1 (Fig. 5f). These findings suggest that K627 is the K63-linked ubiquitination site in RIPK1 that is regulated by OTUD1 and is critical for RIPK1-mediated NF-κB activation.

Studies have reported that NEMO, the regulatory subunit of the IκB kinase (IKK) complex, can be recruited by RIPK1 to induce the activation of the NF-κB signaling pathway [22, 23]. By cotransfecting RIPK1, NEMO and OTUD1 into HEK293T cells, we demonstrated that OTUD1 but not OTUD1 (C320S) attenuated the interaction between RIPK1 and NEMO, suggesting a deubiquitinase activity-dependent role of OTUD1 in inhibiting the RIPK1-NEMO interaction (Supplementary Fig. 6h). Given that OTUD1 could remove K63-linked ubiquitin chains from RIPK1, we postulated that the K63-linked ubiquitin chains on RIPK1 might function as a scaffold to recruit NEMO. To test this hypothesis, coimmunoprecipitation assays were performed with an anti-RIPK1 antibody, and the results showed that OTUD1 inhibited the recruitment of NEMO by RIPK1 during LPS stimulation (Fig. 5g). In addition, the K627R mutant of RIPK1 exhibited a decreased ability to interact with NEMO (Fig. 5h). Furthermore, we demonstrated that the RIPK1 K627R mutant exhibited an increased ability to interact with NEMO during LPS stimulation (Fig. 5i). These results indicate that OTUD1 suppresses the activation of the NF-κB signaling pathway by inhibiting the interaction between RIPK1 and NEMO.

Although multiple DUBs have been shown to regulate the NF-κB signaling pathway by binding to RIPK1, the results of our luciferase assays demonstrated that compared with other DUBs, OTUD1 had the most potent inhibitory effect on RIPK1-mediated activation of the NF-κB pathway (Supplementary Fig. 7). Collectively, these results indicate that OTUD1 inhibits NF-κB signaling by specifically cleaving K63-linked ubiquitin chains on RIPK1 to suppress the recruitment of NEMO.

Mutation of OTUD1 is closely related to human UC

To further confirm the role of OTUD1 in the development of human colitis, we analyzed publicly available UC microarray datasets and found that the expression of OTUD1 in mucosa samples from inflammatory bowel disease patients was usually lower than that in healthy controls (Fig. 6a). The data suggested that OTUD1 is associated with intestinal immune disorders. Several mutations in OTUD1 were observed in patients with autoimmune disorders [8], and OTUD1 mutations frequently occurred in the OTU domain, which is responsible for the deubiquitinating activity of DUBs (Fig. 6b). Similar to OTUD1 C320S, the OTUD1 G430V mutant failed to deubiquitinate RIPK1 (Fig. 6c). Accordingly, G430V lost the ability to inhibit RIPK1-mediated activation of the NF-κB signaling pathway (Fig. 6d). Furthermore, WT *Otud1*, *Otud1* C293S (corresponding to C320 in human OTUD1) and *Otud1* G403V (corresponding to G430 in human OTUD1) were overexpressed in *Otud1*$^{-/-}$ bone marrow-derived cells (BMDMs) through lentiviral transduction, and the data showed that OTUD1 G403V lost the ability to inhibit the activation of the NF-κB signaling pathway (Supplementary Fig. 8a–d). To further verify the role of OTUD1 and its mutants in vivo, BMDMs from *Otud1*$^{-/-}$ mice were infected with lentivirus expressing WT *Otud1*, *Otud1* C293S or *Otud1* G403V and were then transplanted into donor mice. The results obtained in our colitis model indicated that OTUD1 G403V lost the ability to inhibit proinflammatory cytokine production and intestinal inflammation (Fig. 6e–i). Taken together, these findings indicate that OTUD1 maintains immune homeostasis by specifically deubiquitinating RIPK1 (Fig. 7).

DISCUSSION

Studies have revealed that ubiquitination mediated by a number of E3s plays a critical role in activating immune signaling cascades in response to infection and inflammatory signals, while deubiquitination mediated by several DUBs has been shown to prevent exaggerated damaging inflammation [24]. Studies have reported that OTUD1 is involved in the host immune response to pathogen infection by deubiquitinating interferon regulatory factor 3 (IRF3), Smad ubiquitylation regulatory factor-1 (Smurf1), or caspase recruitment domain family member 9 (CARD9) [9, 10, 25]. Recently, OTUD1 was revealed to be the deubiquitinase of iron-responsive element-binding protein 2 (IREB2), which enhances iron transport and potentiates host antitumor immunity [11]. In this study, we found that elevated expression of OTUD1 could be induced by LPS treatment or EPEC infection. Knockdown or deletion of OTUD1 promoted proinflammatory cytokine production. Thus, OTUD1 is a crucial regulator that maintains immune homeostasis by controlling inflammatory responses.

Several DUBs have been shown to contribute to the pathogenesis of IBD by altering the phenotype and function of intestinal cells. TNFAIP3 promotes NF-κB pathway-mediated intestinal epithelial cell (IEC) death to disrupt the intestinal epithelial cell barrier [26]. TNFAIP3 also inhibits the activation of dendritic cells in both MyD88-dependent and MyD88-dependent manners to prevent colitis [7]. In addition, conserved cylindromatosis (CYLD) regulates SMAD-dependent transforming growth factor-β (TGF-β) signaling in effector T cells and regulatory T cells (Tregs) to result in severe spontaneous colitis [27]. During colitis, intestinal

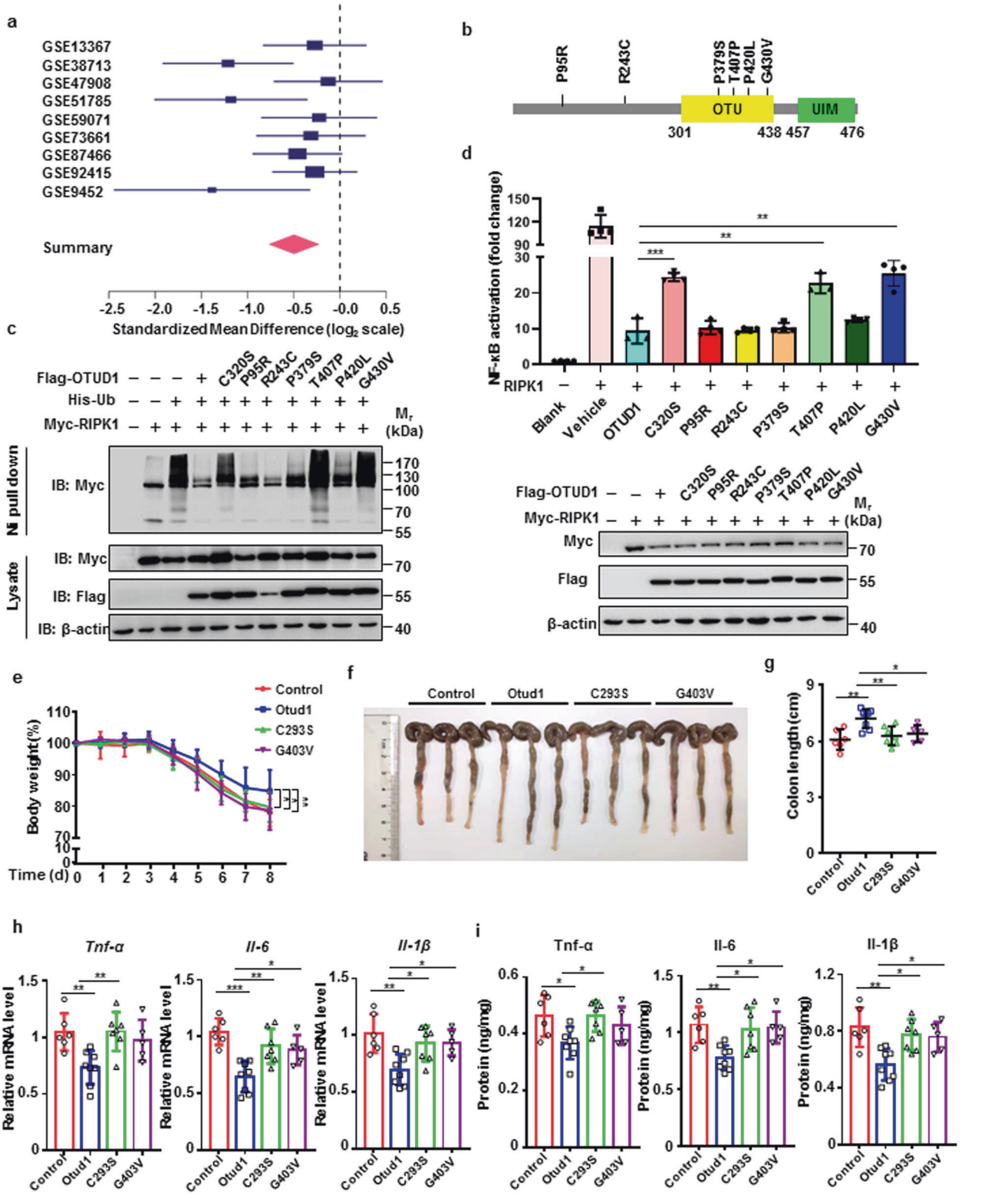

Fig. 6 OTUD1 is associated with human UC. **a** The expression of OTUD1 in human colon mucosa samples. The size of the blue rectangles is proportional to the SEM in the study. **b** Mapping of various mutated sites in OTUD1. **c** Immunoblot analysis of RIPK1 polyubiquitination in cells transfected with Flag-OTUD1 or Flag-tagged OTUD1 mutants. **d** Luciferase assay to evaluate the effects of OTUD1 or OTUD1 mutants on RIPK1-mediated activation of the NF-κB pathway. **e** Body weight of bone marrow chimeric mice exposed to 2.5% DSS for 6 days and then provided regular drinking water for 2 days. **f**, **g** The colon length in bone marrow chimeric mice at Day 8 after initiation of DSS administration. **h** Quantitative PCR analysis of *Il-6*, *Il-1b*, and *Tnf-α* mRNA expression in colon sections from bone marrow chimeric mice treated with 2.5% DSS. **i** ELISA of the production of Il-6, Il-1b, and Tnf-α in colon sections from bone marrow chimeric mice treated with 2.5% DSS. Control, $n = 6$; Otud1, $n = 8$; Otud1 C293S, $n = 7$; Otud1 G403V, $n = 5$. The graph shows a representative mean ± SD of three or four independent biological replicates. $^{*}P < 0.05$; $^{***}P < 0.001$; n.s not significant

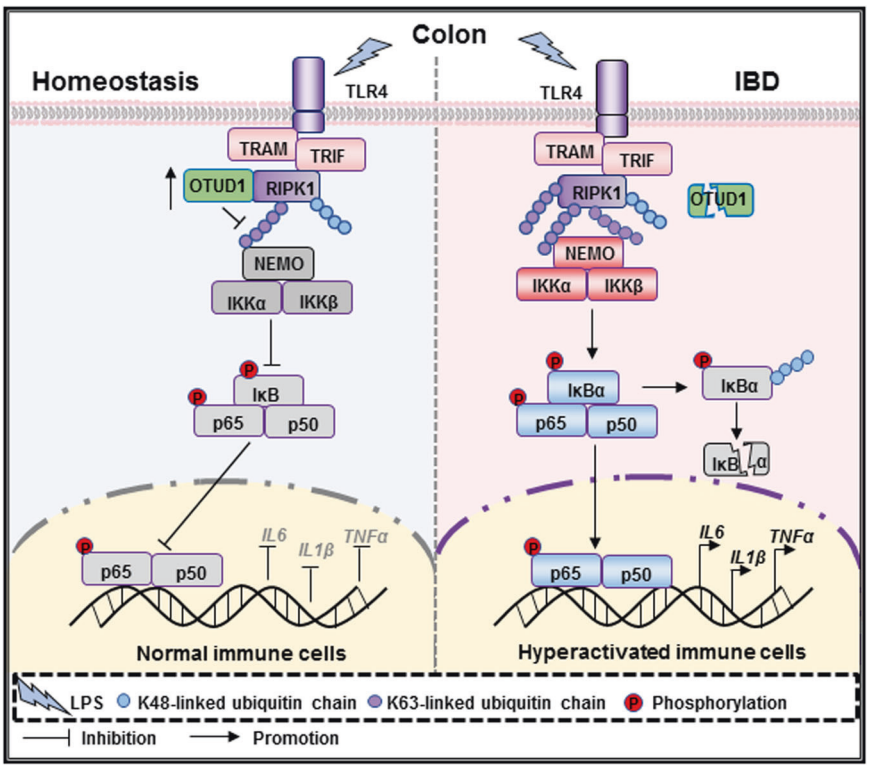

Fig. 7 Proposed model in which the deubiquitinase OTUD1 inhibits DSS-induced colitis by suppressing RIPK1-mediated activation of the NF-κB pathway. Upon DSS treatment, OTUD1 expression is upregulated, which subsequently inhibits K63-linked polyubiquitination of RIPK1 and suppresses the recruitment of NEMO to prevent excessive production of proinflammatory cytokines. When OTUD1 is deleted or mutated, RIPK1 is overmodified by K63-linked ubiquitination at lysine 627, which leads to hyperactivation of the NF-κB signaling pathway in immune cells and eventually results in intestinal inflammation

epithelial cells and immune cells located in the lamina propria can produce various cytokines and other soluble factors to maintain gut homeostasis [28, 29]. For example, intestinal macrophages have been identified to have a tolerant phenotype that supports tolerance to different antigens via overproduction of IL-10 and decreased production of inflammatory cytokines [30]. In this study, we observed upregulated expression of OTUD1 in the colons of mice administered DSS, and the level of OTUD1 in mucosa samples from UC patients was lower than that in mucosa samples from healthy controls. Moreover, *Otud1*$^{-/-}$ mice were more susceptible to exacerbation of colitis with massive leukocyte infiltration into the colon. In addition, *Otud1*$^{-/-}$ mice subjected to DSS-induced colitis produced greater amounts of proinflammatory cytokines, including TNF, IL-6, and IL-1β, than WT mice. Furthermore, OTUD1 in hematopoietic cells was found to play a dominant role in suppressing DSS-induced colitis by inhibiting the production of proinflammatory cytokines. Therefore, OTUD1 deficiency in hematopoietic cells promotes inflammatory responses, thus exacerbating the progression of colitis.

The NF-κB pathway is one of the transcriptional pathways with the highest levels of ubiquitination among its components [31]. Hyperactivation of intestinal immune cells, caused by excessive NF-κB signaling pathway activity and the production of large amounts of proinflammatory cytokines, results in damage to colonic tissue [32]. RIPK1 is a critical NF-κB signaling molecule that controls inflammatory signaling and cell survival through its scaffolding and kinase-specific functions [23]. Patients with biallelic RIPK1 deficiency present with intestinal inflammation and impaired lymphocyte function [33]. Targeting RIPK1 is considered to be an attractive therapeutic strategy for IBD. Several studies have revealed an essential role of RIPK1 in maintaining intestinal epithelial homeostasis, and an imbalance in this process results in IBD [26, 34, 35], but the potential regulatory role of RIPK1 in innate immune cells during the development of intestinal inflammation remains unknown. Our data show that OTUD1 with mutations related to autoimmune diseases (such as systematic lupus erythematosus, ulcerative colitis, rheumatoid arthritis, or Hashimoto's thyroiditis) and located in the OTU domain of OTUD1 cannot inhibit RIPK1 ubiquitination and NF-κB signaling activation [20], indicating that OTUD1 suppresses the RIPK1-activated NF-κB signaling pathway in a deubiquitination activity-dependent manner. Our bone marrow transplantation experiment further revealed that the UC-associated OTUD1 G403V mutant lost the ability to suppress the NF-κB signaling pathway, resulting in more severe intestinal inflammation upon DSS treatment in vivo. By systematic screening with a luciferase reporter assay and IP-MS, we confirmed that OTUD1 suppresses NF-κB signaling through deubiquitination of RIPK1 and that the Ala-rich domain of OTUD1 is crucial for its interaction with the kinase domain of RIPK1. Previous studies have reported that the RIPK1 K377 residue is required for TNF-α-induced NF-κB activation [23], while the K627 residue in RIPK1 mediates opposite effects in response to TNF-α or Toll-like receptor (TLR) stimulation [36]. Here, we demonstrate that OTUD1 specifically reverses K63-linked ubiquitination of RIPK1 at Lys627 and inhibits the recruitment of NEMO, leading to inhibition of the NF-κB signaling pathway. Thus, targeting the OTUD1-RIPK1 axis could be a potential strategy for the treatment of IBD.

In summary, our study reveals that OTUD1 in hematopoietic cells exhibits an inhibitory effect on RIPK1-mediated NF-κB activation to prevent intestinal inflammation by specifically reversing K63-linked ubiquitination of RIPK1 and suppressing the recruitment of NEMO. Our data uncover a crucial role of OTUD1 in maintaining colonic homeostasis by controlling inflammatory responses, suggesting that targeting OTUD1 might be a potential

therapeutic approach for chronic intestinal inflammatory diseases such as IBD.

MATERIALS AND METHODS

Ethics statement

Mice were described previously [10]. In accordance with the "Guide for the Care and Use of Laboratory Animals" and the "Principles for the Utilization and Care of Vertebrate Animals," animal experiments were performed and approved by the Experimental Animal Ethical Committee at Beijing Institute of LifeOmics.

Regents and plasmids

The antibodies used in this study were as follows: anti-OTUD1 (Abcam, #122481), anti-RIPK1 (CST, #3493; BD Biosciences, #610459), anti-p65 (CST, #8242), anti-phospho-p65 (Ser536) (CST, #3031), anti-IκBα (CST, #4814), anti-NEMO (CST, #2695), anti-K48-linkage specific polyubiquitin (CST, #12805), anti-K63-linkage specific polyubiquitin (CST, #12930), anti-phospho-IκBα (CST, #2859), anti-Myc (MBL, #M047-3), anti-DDDDK (MBL, #M185-3L), anti-Ub (MBL, #D058-3), anti-HA (MBL, #M180-3), anti-GFP (Proteintech, #50430-2-AP), and anti-actin (ABclonal, #AC026). Poly(I: C) HMW (tlrl-pic, PIC-41-06) was obtained from InvivoGen. LPS (L7895) was obtained from Sigma–Aldrich. TNF-α (C082) was obtained from Novoprotein.

The vectors encoding MyD88, TRIF, RIPK1, IRAK1, IKKα, IKKβ, TAK1, and TAB2, as well as the plasmids encoding various DUBs and the plasmids expressing ubiquitin lysine-to-arginine mutants, were maintained in our laboratory [37, 38]. The NF-κB-dependent firefly luciferase reporter plasmid, pCMV promoter-dependent Renilla luciferase reporter plasmid, and the plasmid encoding TAB1 were described previously [39]. IKKβ was kindly provided by Dr. Jian Wang (Beijing Institute of LifeOmics). Truncations of OTUD1 and mutants of OTUD1 were constructed using the Gibson Assembly® strategy.

The promoter (−1900/+359 bp) region of OTUD1 was amplified from genomic DNA of U937 cells and was then cloned into the pGL3 vector to generate pGL3-OTUD1. Before transfection, plasmids were methylated in vitro using CpG Methyltransferase (M.SssI, M0226S, NEB) following the manufacturer's instructions.

Cell culture

U937 (ATCC, CRL-3253) and THP-1 (ATCC, TIB-202) cells were cultured in RPMI-1640 medium supplemented with 10% (v/v) fetal calf serum and 2 mM glutamine with penicillin (100 U/mL)/streptomycin (100 mg/mL). U937 cells and THP-1 cells were first treated with 0.5 μM phorbol 12-myristate 13-acetate (PMA, InvivoGen, 16561-29-8) for 16–24 h and then washed once with PBS and cultured in fresh RPMI 1640 medium for an additional 48 h for differentiation into macrophages. 293/hTLR4A-MD2-CD14 cells (InvivoGen, 15B09-MM) were cultured in DMEM supplemented with 4.5 g/L glucose, 10% (v/v) fetal bovine calf serum, penicillin (100 U/mL)/streptomycin (100 mg/mL), Normocin™ (100 μg/mL), blasticidin (10 μg/mL), Hygromycin B Gold (50 μg/mL), and 2 mM L-glutamine. Cells were grown at 37 °C in a humidified incubator with 5% CO_2. BMDMs extracted from femora and tibiae of adult mice were cultured for 6 days in DMEM High Glucose supplemented with 10% (v/v) fetal bovine serum and 2 mM glutamine with penicillin (100 U/mL)/streptomycin (100 mg/mL) and M-CSF (10 ng/mL, Sino Biological, 51112-M08H).

Generation of stable mammalian cell lines

Stable *OTUD1* knockdown cell lines were generated using a lentiviral shRNA technique. Briefly, shRNA targeting human *OTUD1* (1#: TTCAAACTTGCTAGTAGATTTCTC, 2#: CTGAATGTGAATATCCATTTACTC) was cloned into the lentiviral vector pRRLSIN-cPPT-U6-shRNA-SFFV-EGFP-SV40-puromycin to generate the *OTUD1* sh1 and *OTUD1* sh2 vectors, respectively. After lentiviral packaging (GeneChem, Shanghai, China), U937 cells were infected with lentivirus in the presence of 4 mg/mL polybrene and selected with 2 μg/mL puromycin for at least 7 days before additional experiments were performed.

Bacterial infection

Escherichia coli (EPEC) cells were cultured in Luria–Bertani (LB) medium supplemented with 50 ng/mL nalidixic acid sodium salt (NAL) (Sigma, N4382). For infection, U937 cells and THP-1 cells were differentiated by incubation with 0.5 μM phorbol 12-myristate 13-acetate (PMA, InvivoGen, 16561-29-8) for 16–24 h in a 6-well plate, washed once with PBS, cultured in fresh RPMI 1640 medium for an additional 48 h and then infected with EPEC at a multiplicity of infection (MOI) of 150 for 1–2 h. The cells were then washed three times with PBS to remove extra bacteria and harvested for further analysis.

Quantitative PCR (qPCR)

Total RNA was extracted with TRIzol (Invitrogen). Total RNA (1 μg) was reverse transcribed into cDNA using ReverTra Ace™ qPCR Master Mix (FSQ-201, Toyobo). Quantitative real-time PCR was carried out using 2 × RealStar Green Fast Mixture (A301, GenStar, Beijing, China) and specific primers in a real-time PCR instrument (Roche, LightCycler *R* 96). Data were analyzed as previously reported [40]. The primers used to obtain the indicated gene products are described in Supplementary Table 1.

Methylation-specific PCR

After U937 cells were treated with LPS for 1 h, genomic DNA was isolated using a Genome Extraction Kit (DP304, TIANGEN, China). Bisulfite modification of DNA was performed using a DNA Methylation Bisulfite Kit (EM101-01, Vazyme, China) according to the manufacturer's instructions. To analyze the methylation of OTUD1 DNA, methylation-specific PCR was performed using 2 × EpiArt® HS Taq Master Mix (EM201, Vazyme, China). PCR products were separated on a 2% agarose gel, stained with SYBR Safe DNA Gel Stain (S33102, Thermo Fisher Scientific, USA), and visualized with a FluorChem R System (Protein Simple). The primer sets were designed using the MethPrimer program and were as follows: unmethylated forward, 5′- AGGAT TTTAGGATTGTTTAGGTTTTT-3′ and unmethylated reverse, 5′- TAAAATACA CAACTCTTTACAACACC-3′; methylated forward, 5′- GGATTTTAGGATTGTT TAGGTTTTC-3′ and methylated reverse, 5′- ATACGCGACTCTTTACGACG -3′.

DSS-induced colitis model

The DSS-induced colitis model was established as previously described [41]. Briefly, WT and *Otud1*$^{-/-}$ mice (female, 6–8 weeks old) were treated with 2.5% DSS (MW 36,000–50,000 Da; MP Biomedicals, MP-0216011050) in the drinking water for 6 days and were then provided regular water for another 2 days. Body weight loss was monitored daily, and rectal bleeding was scored as follows: 0, absence of blood on the Hemoccult test (Beckman Coulter); 1, positive Hemoccult test; 2, visible blood traces in stool; and 3, gross rectal bleeding. The entire colon was excised for measurement of the colon length on Day 8. Then, freshly isolated distal colons were fixed with 4% paraformaldehyde and embedded in paraffin, and tissue sections were stained with hematoxylin & eosin (H&E). Histological scoring was performed by a pathologist in a blinded manner, as described previously [42].

Bone marrow transplantation experiments

Recipient mice were irradiated with two doses of 5.5 Gy γ-radiation and injected i.v. with donor BM cells (4×10^6 cells per mouse). Recipient mice were maintained for 2 weeks on water containing trimethoprim-sulfamethoxazole. Six weeks after BM transplantation, mice were challenged with DSS. Body weights and rectal bleeding were monitored daily.

Lentivirus infection

The recombinant OTUD1, OTUD1 (C320S), OTUD1 (G430V) and negative control lentiviruses were purchased from Shanghai Jikai Company (Shanghai, China). Bone marrow-derived cells were infected with lentiviruses for 12 h and transplanted into lethally irradiated mice.

Isolation of lymphocytes from the intestinal lamina propria and mesenteric lymph nodes

Intestines were harvested from mice, and Peyer's patches were removed. Intestines were cut into small pieces and thoroughly washed with ice-cold PBS solution. Epithelial cells were removed by incubating intestinal tissues in Hank's balanced salt solution supplemented with 1 mM EDTA and 1 mM DTT at 37 °C for 30 min with gentle shaking, followed by extensive washing with PBS. Residual tissues were then digested with collagenase II (YEASEN), collagenase III (YEASEN) and DNase I (YEASEN) at 37 °C for 60 min with gentle shaking. Cells from colons and mesenteric lymph nodes were isolated and filtered through a 70-μm cell strainer (BD Biosciences) and stained for flow cytometric analysis.

Immune cell populations were defined by antibody staining as follows: macrophages ($CD45^+CD11b^+F4/80^+$), NK cells ($CD45^+NK1.1^+$), B cells ($CD45^+B220^+$), neutrophils ($CD45^+CD11b^+Ly6G^+$), DCs ($CD45^+CD11c^+$), $CD4^+$ T cells ($CD45^+CD3^+CD4^+$), $CD8^+$ T cells ($CD45^+CD3^+CD8^+$), Th1 cells ($CD45^+CD3^+CD4^+IFN\text{-}\gamma^+IL\text{-}17A^-$), Th17 cells ($CD45^+CD3^+CD4^+IFN\text{-}\gamma^-IL\text{-}17A^+$), and Th1/Th17 cells ($CD45^+CD3^+CD4^+IFN\text{-}\gamma^+IL\text{-}17A^+$). $CD4^+$ and $CD8^+$ subsets were classified as naïve T (T_N) cells ($CD62L^+CD44^-$), effector memory T (T_{EM}) cells ($CD62L^-CD44^+$) and central memory T (T_{CM}) cells ($CD62L^+CD44^+$). Data were acquired on an LSRFortessa cell analyzer (BD Biosciences) and analyzed with FlowJo software (TreeStar). Cell sorting was performed on a BD Influx cell sorter (BD Biosciences).

Immunofluorescence staining

Immunofluorescence staining was performed as previously described. Briefly, cells cultured on 24-mm diameter cover slips were fixed, permeabilized with 0.2% Triton X-100 and incubated first with primary antibodies overnight at 4 °C and then with secondary antibodies conjugated to Alexa Fluor 488 or 594 (Zhongshan Golden Bridge). Cells were counterstained with 4′,6-diamidino-2-phenylindole to visualize nuclei. Confocal images were acquired with a Leica SP8 confocal microscope system.

Enzyme-linked immunosorbent assay (ELISA)

BMDMs were seeded (2×10^6 cells/well) in a 6-well plate and treated with LPS (100 ng/mL) for 8 h. After incubation, the medium was collected and used for ELISA. According to the manufacturer's instructions, the concentrations of mouse Il-6, Il-1b, and Tnf-α in cell supernatants were measured using commercial ELISA kits (Boster, Wuhan, China).

Dual-luciferase reporter assay

Plasmids encoding MyD88, IRAK1, TRIF, RIPK1, IKKα, TAK1/TAB2 or OTUD1, were transfected together with NF-κB promoter-driven firefly luciferase (NF-κB reporter) and CMV-driven Renilla luciferase vectors into HEK293T cells for 36 h using Lipofectamine 2000 (Invitrogen) reagent according to the manufacturer's protocol. According to the manufacturer's instructions, luciferase activity was assessed luminometrically by using a dual-luciferase assay system (Promega, Madison, WI, USA).

Immunoprecipitation and immunoblotting

Cells were lysed with NP40 lysis buffer (50 mM Tris-HCl (pH 8.0), 150 mM NaCl, 1% NP40, 0.5% deoxycholate) supplemented with a protease inhibitor cocktail (HY-K0010, MCE) on ice before sonicating for 1 min After centrifugation at 12,000 × g for 15 min, the supernatant was incubated sequentially with the indicated primary antibody for 1 h and with protein A/G agarose beads (sc-2003, Santa Cruz) overnight on a rotator at 4 °C. The immunocomplexes were washed with 800 μl of lysis buffer three times and boiled with 2 × loading buffer for 5 min Both the lysates and immunoprecipitates were subjected to immunoblotting using the indicated primary antibodies (Jackson, United States).

Glutathione S-transferase (GST) pulldown assay

Full-length human OTUD1 cDNA was cloned into the pGEX-4T-2 vector with an N-terminal GST tag. GST and GST-OTUD1 proteins were obtained by expression in a prokaryotic expression system. HEK293T cells cultured in 10-cm^2 dishes were collected and lysed with NP40 buffer containing protease inhibitor cocktail. Then, the supernatant was collected after centrifugation at 12,000 × *g* for 15 min Furthermore, GST and GST-OTUD1 proteins bound to Glutathione-Sepharose 4B beads (GE) were incubated with HEK 293T cell supernatant overnight at 4 °C on a rotator. Then, the beads were washed with NP40 buffer four times for further analysis by immunoblotting.

Mass spectrometry analysis

Flag-OTUD1 was immunoprecipitated from lysates of Flag-OTUD1-overexpressing HEK293T cells with anti-Flag antibodies or normal mouse IgG as described above. The immunoprecipitates were separated by SDS–PAGE, and the gels were stained with Coomassie Blue. Proteins interacting with OTUD1 were identified by mass spectrometry as previously described [38]. A Q-Exactive HF MS system (Thermo Fisher Scientific) connected to an online Easy-nLC 1200 nano-HPLC system (Thermo Fisher Scientific) was used to analyze the samples obtained by in-gel digestion. The dried peptide samples were resuspended in 12 μL of solvent A (0.1% formic acid in water), and 5 μL of each sample was then loaded onto a 2 cm in-house-packed trap column (100 μm inner diameter, 3 μm resin; ReproSil-Pur C18-AQ, Dr. Maisch GmbH). After the loading and washing steps, peptides were transferred to a 15 cm column (150 μm inner diameter, 1.9 μm resin; ReproSil-Pur C18-AQ, Dr. Maisch GmbH) and separated over 75 min on a nonlinear gradient from 4% to 95% solvent B (0.1% FA in ACN) at a flow rate of 600 nL/min. Peptides were ionized using a 2.0 kV electrospray voltage and a capillary temperature of 320 °C. Data acquisition was performed in OT–OT mode. Full MS scans (300 to 1400 m/z) were performed at a resolution of 120,000, a maximum injection time of 80 ms, and an AGC target of 3e6. Tandem mass spectra were generated for up to 30 precursors by HCD with a normalized collision energy of 27%. Dynamic exclusion was set to 15 s. The MS2 spectra were acquired in the Orbitrap at a resolution of 15,000 with an AGC target of 5e4 and a maximum injection time of 20 ms. The acquired MS/MS spectra were searched against the human National Center for Biotechnology Information (NCBI) RefSeq protein databases (updated on April 7, 2013; 32,015 protein entries) with Mascot 2.3 (Matrix Science Inc, MA) implemented in Proteome Discoverer 2.1 (Thermo). The mass tolerances were 20 ppm for precursor ions and 50 mmu for product ions. Peptides and proteins were filtered with a false discovery rate of 1% using the decoy database strategy. The minimal peptide length was seven amino acids. Protein identification data (accession numbers, peptides observed, sequence coverage) are available in Supplementary Table 2.

In vitro ubiquitination assay

For the in vitro ubiquitination assay, Myc-RIPK1 and His-Ub, together with WT or CS mutant Flag-OTUD1, were transfected into HEK293T cells for 24 h. Then, the cells were treated with the proteasome inhibitor MG132 (20 μM; HY-13259, MCE) for another 6 h. Then, the cells were lysed under denaturing conditions (buffer A: 6 M guanidine-HCl, 100 mM sodium phosphate, 10 mM imidazole (pH 8.0)) on ice. After sonication for 2 min and centrifugation at 12,000 × g for 15 min, the supernatant was incubated with nickel-nitrilotriacetic acid (Ni-NTA) matrices (QIAGEN) for 3 h. Then, the His-tag pulldown products were washed sequentially once in buffer A, twice in a buffer A/buffer TI mixture (buffer A:buffer TI = 1:3), and once in buffer TI (25 mM Tris-HCl and 20 mM imidazole (pH 6.8)) to purify the polyubiquitinated proteins at room temperature. The polyubiquitinated proteins were separated by SDS–PAGE and subjected to immunoblotting with an anti-Myc monoclonal antibody. Similarly, HEK293T cells transfected with Myc-RIPK1 along with WT, K0-linked, K6-linked, K11-linked, K27-linked, K33-linked, K48-linked or K63-linked HA-tagged Ub, and Flag-OTUD1 were lysed with RIPA lysis buffer (50 mM Tris-HCl (pH 7.4), 150 mM NaCl, 5 mM EDTA, 0.5% sodium deoxycholate, and 1% Triton X-100). Proteins were immunoprecipitated with anti-Myc antibody for 3 h and incubated with protein A/G agarose beads on a rotator overnight at 4 °C. Then, the beads were washed three times with RIPA lysis buffer and subjected to immunoblotting with an anti-HA monoclonal antibody.

In vitro deubiquitination assay

U937 cells were stimulated with 100 ng/ml LPS for 2 h and were then lysed with IP lysis buffer containing 20 mM Tris-HCl (pH 7.4), 150 mM NaCl, 2.5 mM EDTA, 1% (v/v) Triton X-100, EDTA-free complete protease inhibitor, 100 mM NaF, 5 mM N-ethylmaleimide (NEM) and 10 mM iodoacetamide. The RIPK1 protein was captured with an anti-RIPK1 antibody and agarose beads as described above. Beads linked to RIPK1 were washed three times with 1 ml of IP wash buffer containing 20 mM Tris-HCl (pH 7.4), 150 mM NaCl, 2.5 mM EDTA, 1% (v/v) Triton X-100 and EDTA-free complete protease inhibitor. Subsequently, the beads were resuspended in 40 μl of DUB dilution buffer (50 mM Tris-HCl (pH 7.5), 100 mM NaCl, 2 mM DTT, 1 mM MnCl2, and 0.01% (w/v) Brij 35) with λ-PPase (100 units/reaction) and incubated for 3 h at 37 °C with purified GST or GST-OTUD1/OTUD1-CS/USP21 (Ser196-Leu565). Reactions were terminated by denaturation in 5 × loading buffer, and SDS–PAGE was then performed.

Signaling pathway enrichment analysis

For signaling pathway enrichment analysis, we employed the BioCarta database (http://www.biocarta.com/genes/index.asp) to evaluate the functional pathways of the OTUD1-interacting proteins. Enrichment analysis was carried out using the R clusterProfiler package. For this study, an adjusted $P < 0.05$ was considered to indicate statistically significant enrichment. The top 10 enriched signaling pathways are listed in

Supplementary Table 2 and were visualized using Hiplot (https://hiplot.com.cn/basic/bubble).

Gene expression meta-analysis

Publicly available UC microarray datasets were obtained from the NCBI GEO (Gene Expression Omnibus) database (https://www.ncbi.nlm.nih.gov/geo/) and EBI Array Express database (https://www.ebi.ac.uk/arrayexpress/). The datasets that focused on intestinal tissue and had a UC patient cohort size of >20 were included for further analysis. Each microarray dataset was converted into a gene expression matrix by the limma R package [43]. The Hedges' *g* effect size was then computed to estimate gene expression changes in each dataset. The effect sizes from all individual datasets were integrated into a summary effect size by the Meta Integrator R package [44]. Plots and statistics were generated using the R programming language.

Statistical analysis

All statistical analyses were performed using Prism 8 software. All data were analyzed using unpaired Student's *t* test or one-way or two-way ANOVA with the Bonferroni post hoc test to correct for multiple comparisons, as indicated in the corresponding figure legends. A $P < 0.05$ was considered significant, and the level of significance is indicated as $^{*}P < 0.05$, $^{**}P < 0.01$, and $^{***}P < 0.001$.

REFERENCES

1. Peloquin JM, Goel G, Villablanca EJ, Xavier RJ. Mechanisms of pediatric inflammatory bowel disease. Annu Rev Immunol. 2016;34:31–64.
2. Peterson LW, Artis D. Intestinal epithelial cells: regulators of barrier function and immune homeostasis. Nat Rev Immunol. 2014;14:141–53.
3. Cleynen I, Vazeille E, Artieda M, Verspaget HW, Szczypiorska M, Bringer MA, et al. Genetic and microbial factors modulating the ubiquitin proteasome system in inflammatory bowel disease. Gut. 2014;63:1265–74.
4. Xiao Y, Huang Q, Wu Z, Chen W. Roles of protein ubiquitination in inflammatory bowel disease. Immunobiology. 2020;225:152026.
5. Neurath MF. Cytokines in inflammatory bowel disease. Nat Rev Immunol. 2014;14:329–42.
6. van Loosdregt J, Fleskens V, Fu J, Brenkman AB, Bekker CP, Pals CE, et al. Stabilization of the transcription factor Foxp3 by the deubiquitinase USP7 increases Treg-cell-suppressive capacity. Immunity. 2013;39:259–71.
7. Hammer GE, Turer EE, Taylor KE, Fang CJ, Advincula R, Oshima S, et al. Expression of A20 by dendritic cells preserves immune homeostasis and prevents colitis and spondyloarthritis. Nat Immunol. 2011;12:1184–93.
8. Lu D, Song J, Sun Y, Qi F, Liu L, Jin Y, et al. Mutations of deubiquitinase OTUD1 are associated with autoimmune disorders. J Autoimmun. 2018;94:156–65.
9. Chen X, Zhang H, Wang X, Shao Z, Li Y, Zhao G, et al. OTUD1 regulates antifungal innate immunity through deubiquitination of CARD9. J Immunol. 2021;206:1832–43.
10. Zhang L, Liu J, Qian L, Feng Q, Wang X, Yuan Y, et al. Induction of OTUD1 by RNA viruses potently inhibits innate immune responses by promoting degradation of the MAVS/TRAF3/TRAF6 signalosome. PLoS Pathog. 2018;14:e1007067.
11. Song J, Liu T, Yin Y, Zhao W, Lin Z, Yin Y, et al. The deubiquitinase OTUD1 enhances iron transport and potentiates host antitumor immunity. EMBO Rep. 2021;22:e51162.
12. Clague MJ, Urbe S, Komander D. Breaking the chains: deubiquitylating enzyme specificity begets function. Nat Rev Mol Cell Biol. 2019;20:338–52.
13. Akira S, Uematsu S, Takeuchi O. Pathogen recognition and innate immunity. Cell. 2006;124:783–801.
14. Jones PA. Functions of DNA methylation: islands, start sites, gene bodies and beyond. Nat Rev Genet. 2012;13:484–92.
15. Zhang Z, Wang D, Wang P, Zhao Y, You F. OTUD1 negatively regulates type I IFN induction by disrupting noncanonical ubiquitination of IRF3. J Immunol. 2020;204:1904–18.
16. Ashida H, Ogawa M, Kim M, Mimuro H, Sasakawa C. Bacteria and host interactions in the gut epithelial barrier. Nat Chem Biol. 2011;8:36–45.
17. Maes M, Kubera M, Leunis JC. The gut-brain barrier in major depression: intestinal mucosal dysfunction with an increased translocation of LPS from gram negative enterobacteria (leaky gut) plays a role in the inflammatory pathophysiology of depression. Neuro Endocrinol Lett. 2008;29:117–24.
18. Zhang YZ, Li YY. Inflammatory bowel disease: pathogenesis. World J Gastroenterol. 2014;20:91–9.
19. Hoesel B, Schmid JA. The complexity of NF-kappaB signaling in inflammation and cancer. Mol Cancer. 2013;12:86.
20. Hayden MS, Ghosh S. Shared principles in NF-kappaB signaling. Cell. 2008;132:344–62.
21. Zhang Z, Fan Y, Xie F, Zhou H, Jin K, Shao L, et al. Breast cancer metastasis suppressor OTUD1 deubiquitinates SMAD7. Nat Commun. 2017;8:2116.
22. Ea CK, Deng L, Xia ZP, Pineda G, Chen ZJ. Activation of IKK by TNFalpha requires site-specific ubiquitination of RIP1 and polyubiquitin binding by NEMO. Mol Cell. 2006;22:245–57.
23. Li H, Kobayashi M, Blonska M, You Y, Lin X. Ubiquitination of RIP is required for tumor necrosis factor alpha-induced NF-kappaB activation. J Biol Chem. 2006;281:13636–43.
24. Jiang X, Chen ZJ. The role of ubiquitylation in immune defence and pathogen evasion. Nat Rev Immunol. 2011;12:35–48.
25. Wang S, Hou P, Pan W, He W, He DC, Wang H, et al. DDIT3 Targets Innate Immunity via the DDIT3-OTUD1-MAVS Pathway To Promote Bovine Viral Diarrhea Virus Replication. J Virol. 2021;95:e02351–20.
26. Garcia-Carbonell R, Wong J, Kim JY, Close LA, Boland BS, Wong TL, et al. Elevated A20 promotes TNF-induced and RIPK1-dependent intestinal epithelial cell death. Proc Natl Acad Sci USA. 2018;115:E9192–200.
27. Tang Y, Reissig S, Glasmacher E, Regen T, Wanke F, Nikolaev A, et al. Alternative splice forms of CYLD mediate ubiquitination of SMAD7 to prevent TGFB signaling and promote colitis. Gastroenterology. 2019;156:692–707 e697.
28. Bain CC, Mowat AM. Macrophages in intestinal homeostasis and inflammation. Immunol Rev. 2014;260:102–17.
29. Na YR, Stakenborg M, Seok SH, Matteoli G. Macrophages in intestinal inflammation and resolution: a potential therapeutic target in IBD. Nat Rev Gastroenterol Hepatol. 2019;16:531–43.
30. Moreira Lopes TC, Mosser DM, Goncalves R. Macrophage polarization in intestinal inflammation and gut homeostasis. Inflamm Res. 2020;69:1163–72.
31. Wullaert A. Role of NF-kappaB activation in intestinal immune homeostasis. Int J Med Microbiol. 2010;300:49–56.
32. Atreya I, Atreya R, Neurath MF. NF-kappaB in inflammatory bowel disease. J Intern Med. 2008;263:591–6.
33. Li Y, Fuhrer M, Bahrami E, Socha P, Klaudel-Dreszler M, Bouzidi A, et al. Human RIPK1 deficiency causes combined immunodeficiency and inflammatory bowel diseases. Proc Natl Acad Sci USA. 2019;116:970–5.
34. Dannappel M, Vlantis K, Kumari S, Polykratis A, Kim C, Wachsmuth L, et al. RIPK1 maintains epithelial homeostasis by inhibiting apoptosis and necroptosis. Nature. 2014;513:90–4.
35. Takahashi N, Vereecke L, Bertrand MJ, Duprez L, Berger SB, Divert T, et al. RIPK1 ensures intestinal homeostasis by protecting the epithelium against apoptosis. Nature. 2014;513:95–9.
36. Li X, Zhang M, Huang X, Liang W, Li G, Lu X, et al. Ubiquitination of RIPK1 regulates its activation mediated by TNFR1 and TLRs signaling in distinct manners. Nat Commun. 2020;11:6364.
37. Li S, Lu K, Wang J, An L, Yang G, Chen H, et al. Ubiquitin ligase Smurf1 targets TRAF family proteins for ubiquitination and degradation. Mol Cell Biochem. 2010;338:11–7.
38. Du T, Li H, Fan Y, Yuan L, Guo X, Zhu Q, et al. The deubiquitylase OTUD3 stabilizes GRP78 and promotes lung tumorigenesis. Nat Commun. 2019;10:2914.
39. Wang J, Li B-X, Ge P-P, Li J, Wang Q, Gao GF, et al. Mycobacterium tuberculosis suppresses innate immunity by coopting the host ubiquitin system. Nat Immunol. 2015;16:237–45.
40. Université Clermont Auvergne IUNHUdNHCAFC-FF, Tournayre J, Reichstadt M, Parry L, Fafournoux P, Jousse C. "Do my qPCR calculation", a web tool. Bioinformation. 2019;15:369–72.
41. Liu Z-Y, Wu B, Guo Y-S, Zhou Y-H, Fu Z-G, Xu B-Q, et al. Necrostatin-1 reduces intestinal inflammation and colitis-associated tumorigenesis in mice. Am J Cancer Res. 2015;5:3174.
42. Zaki MH, Boyd KL, Vogel P, Kastan MB, Lamkanfi M, Kanneganti TD. The NLRP3 inflammasome protects against loss of epithelial integrity and mortality during experimental colitis. Immunity. 2010;32:379–91.
43. Ritchie ME, Phipson B, Wu D, Hu Y, Law CW, Shi W, et al. limma powers differential expression analyses for RNA-sequencing and microarray studies. Nucleic Acids Res. 2015;43:e47–7.
44. Khatri P, Roedder S, Kimura N, Vusser KD, Morgan AA, Gong Y, et al. A common rejection module (CRM) for acute rejection across multiple organs identifies novel therapeutics for organ transplantation. J Exp Med. 2013;210:2205–21.

ACKNOWLEDGEMENTS

We thank Ke Zhao (State Key Laboratory of Proteomics, National Center for Protein Sciences (Beijing), Beijing Institute of LifeOmics, Beijing) for technical assistance in the mouse transplantation experiments and Tong Zhao (Institute of Microbiology, Chinese Academy of Sciences, Beijing) for helping with the flow cytometry data generation and analysis.

AUTHOR CONTRIBUTIONS

CHL and LZ designed the research; BW, LQ, YZ and YF performed most experiments and analyzed the data; MZ, ZL, ML, XZ, ZP, HD, YW, YG and JW also performed experiments; HZ provided the *Otud1*$^{-/-}$ mice; HL helped with the animal experiments; BW, LQ and YZ wrote the paper; CHL and LZ read and approved the final version of the paper.

FUNDING

This work was jointly supported by the National Key Research and Development Project of China (2021YFA1300200), the Biosafety Special Project of China (19SWAQ17), the National Natural Science Foundation of China (31800746, 31830003 and 81825014), the Strategic Priority Research Program of the Chinese Academy of Sciences (XDB29020000) and the State Key Laboratory of Proteomics (SKLP-K202001).

COMPETING INTERESTS

The authors declare no competing interests.

ADDITIONAL INFORMATION

Supplementary information The online version contains supplementary material available at https://doi.org/10.1038/s41423-021-00810-9.

Correspondence and requests for materials should be addressed to Cui Hua Liu or Lingqiang Zhang.